Lawrence Berkeley National Laboratory
Recent Work

Title
THE MECHANISM OF IONIZATION DAMAGE IN GLASSY CERAMICS

Permalink
https://escholarship.org/uc/item/2n77m8c2

Author
Laval, J.Y.

Publication Date
1979-03-01

eScholarship.org Powered by the California Digital Library
University of California

LBL-9008 c.2
Preprint

Lawrence Berkeley Laboratory
UNIVERSITY OF CALIFORNIA

Materials & Molecular Research Division

Submitted to the Journal of the American Ceramic Society

THE MECHANISM OF IONIZATION DAMAGE IN GLASSY CERAMICS

J. Y. Laval and K. H. Westmacott

RECEIVED
LAWRENCE
BERKELEY LABORATORY
NOV 16 1979
LIBRARY AND
DOCUMENTS SECTION

March 1979

TWO-WEEK LOAN COPY

This is a Library Circulating Copy which may be borrowed for two weeks. For a personal retention copy, call Tech. Info. Division, Ext. 6782.

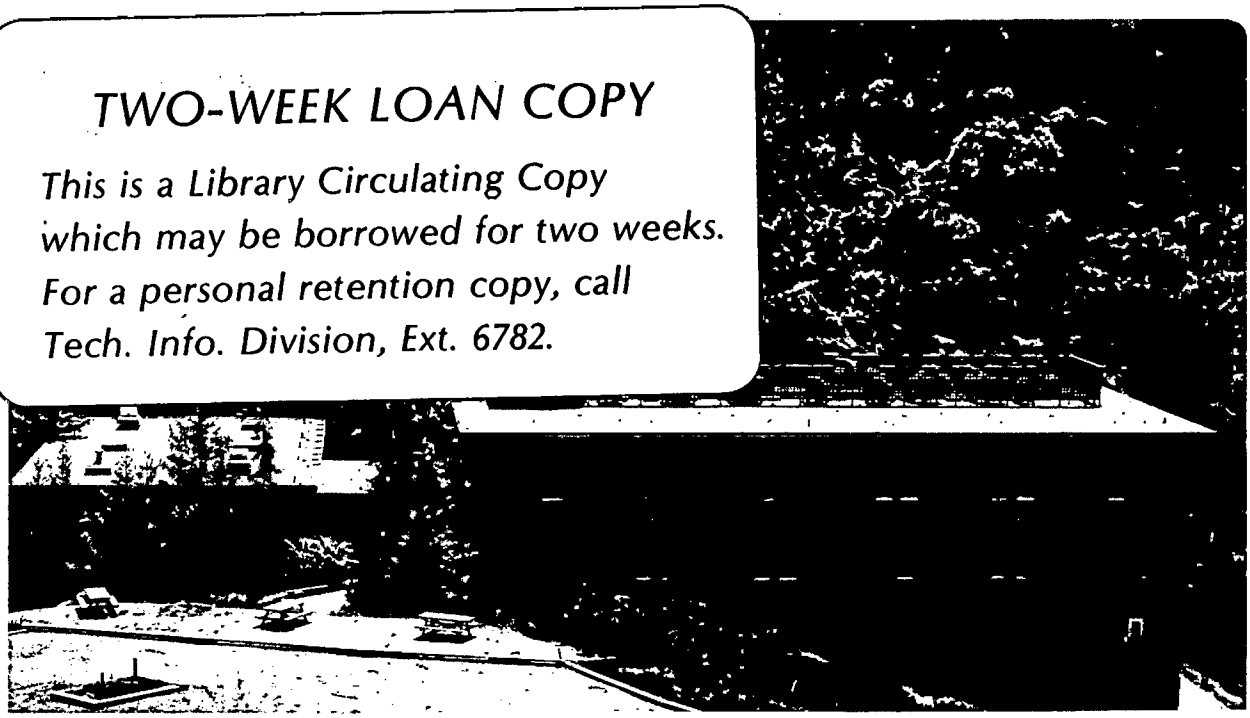

Prepared for the U.S. Department of Energy under Contract W-7405-ENG-48

LBL-9008 c.2

DISCLAIMER

This document was prepared as an account of work sponsored by the United States Government. While this document is believed to contain correct information, neither the United States Government nor any agency thereof, nor the Regents of the University of California, nor any of their employees, makes any warranty, express or implied, or assumes any legal responsibility for the accuracy, completeness, or usefulness of any information, apparatus, product, or process disclosed, or represents that its use would not infringe privately owned rights. Reference herein to any specific commercial product, process, or service by its trade name, trademark, manufacturer, or otherwise, does not necessarily constitute or imply its endorsement, recommendation, or favoring by the United States Government or any agency thereof, or the Regents of the University of California. The views and opinions of authors expressed herein do not necessarily state or reflect those of the United States Government or any agency thereof or the Regents of the University of California.

THE MECHANISM OF IONIZATION DAMAGE IN GLASSY CERAMICS

J. Y. Laval* and K. H. Westmacott

Materials and Molecular Research Division,
Lawrence Berkeley Laboratory

and

Department of Materials Science and Mineral Engineering
University of California, Berkeley, California 94720

ABSTRACT

The structural changes that occur in the glassy phase of certain ceramics during exposure in an electron beam are analyzed in a nitride, ferrite, and oxide. In Si_3N_4 containing MgO, which was investigated in the greatest detail, small void-like defects, postulated to be oxygen gas bubbles, nucleate and grow to diameters in excess of 50 nm. Similar effects are observed in MnZn ferrite and ZnO. The voltage and beam current dependence of the defect growth rate is consistent with an ionization damage process. The results are compared with previous work and a model proposed whereby certain additives or impurities concentrate in the glassy phase, modify the bonding, and increase its sensitivity to ionizing radiation. Free oxygen liberated by electron transfer processes saturates the glass leading to bubble nucleation and growth. The presence of polyvalent elements in the glass can inhibit gas liberation and bubble formation, and the relative amounts and valencies of impurities present will determine its susceptibility to damage.

---

*Chargé de Recherche, Centre National de la Recherche Scientifique, Paris; on leave at Lawrence Berkeley Laboratory.

I. INTRODUCTION

In transmission electron microscopy (TEM) of metallic materials at conventional voltages (100 kV), changes in structures due to the interaction of the electron beam with the specimen can be neglected for two reasons. (1) The energy an atom receives from an electron in a direct nuclear collision is insufficient to displace it from its normal lattice site, and (2) ionization and excitation events resulting from electron interactions with orbital electrons are transient (10^{-15}s long) and cause no permanent structural changes. Electron microscopy at higher accelerating voltages in a high voltage electron microscopy (HVEM) or in non-metals at 100 kV can modify the structure. For organic compounds the damage resulting from ionization and other electronic effects at any voltage imposes severe limitation on the information obtainable from TEM techniques.[1] Alkali and alkali-earth halides are very sensitive to the electron beam.[2] Dislocation loops are formed first, and then the salts decomposed into bubbles (e.g., iodine) and metallic colloids.[3] Glasses exhibit a variety of defects under an electron beam,[4] and defects clustering can lead to the outgassing of oxygen.[5] Ceramics form an interesting intermediate class of materials because of their wide range of bonding properties. Reductions of the cation into metal may occur in an oxide film (e.g., Al_2O_3),[6] at the metal-oxide interface or at the surface (e.g., Cu_2O).[7] Changes in bulk microstructure have been reported in Si_3N_4 and in sialons by Drew and Lewis[8,9] but the effects are confined to intercrystalline glassy phases. Makin[10] observed extensive transformation in microstructure in SiO_2-MgO glasses irradiated in an HVEM and studied the effects as a function of glass composition.

This paper reports an investigation of the mechanism and kinetics of ionization damage in glassy phases in several ceramics (a nitride, spinel, and oxide). We have analyzed the progressive development of structural imperfections under an electron beam for different voltages and intensities and compared the results to previous work. It is proposed that the formation of damage occurs only when certain network modifying additions are present in the glass.

1. Experimental Techniques

The ceramics materials were performed by conventional sintering techniques. CaO and MgO, commonly used sintering additives aid densification as they lower the liquidus temperature of the pure ceramic, giving liquids at sintering temperatures. However, they readily segregate at the grain boundaries as it has been shown by x-ray microanalysis[11] and promote the formation of intergranular glassy phase. The major constituents and processing history for each material are presented in Table I. Specimens suitable for transmission electron microscopy were prepared from thin disks by ion thinning.[12] For the silicon nitride, the specimens were coated with a thin layer of carbon by vapor deposition following the ion thinning to minimize beam-induced charging. Initial microscopy was performed on a Siemens 102 operated at 100 and 125 kV. Subsequently, observations were extended to lower accelerating voltages 60 and 80 kV in the Siemens, and to high voltages in the range 150-650 kV in an Hitachi HU 650.

2. Results

2.1 Damage Nucleation

(i) Silicon nitride

Microstructural examination of the silicon nitride in the electron microscope at 100 kV revealed a fine scale structure of equiaxed grains.

During a short exposure to the electron beam, certain regions of the specimens transformed. Mottled contrast developed, which was restricted to areas surrounding clearly defined grains and to other grain boundary layers (Fig. 1). These regions were subsequently identified as the glassy phase (G). Similar changes were first noted at 200 kV by Drew and Lewis,[8] who suggested that the effects were due to an unidentified irradiation damage process, and could be used for quickly identifying the regions of amorphous phase. A typical sequence showing the nucleation and growth of void-like features is given in Fig. 2. The features always appeared lighter than background in bright field micrographs and vice-versa in dark field. Stereomicroscopy confirmed that the defects were distributed uniformly throughout the thickness of the affected regions (see Fig. 3) and not confined to the surfaces. In some cases the images of defects at different levels superimposed producing a lighter contrast in the overlapping region. The observed contrast features are consistent with the presence of irregular shaped cavities or gas bubbles in the bulk of the glassy phase. In crystalline materials a void or bubble imaged by diffraction contrast may appear dark on a bright background or vice-versa depending on the deviation parameters.[13] In amorphous phases, however, it will be seen only by absorption contrast and thus will always appear lighter than background. We now anticipate later conclusions and hereafter refer to these imperfections as gas bubbles.

(ii) Manganese-Zinc ferrite

The spreading of the glassy phase at the grain boundaries is much more restricted for manganese-zinc ferrite fluxed with CaO than for silicon nitride. The glassy phase is mostly limited to triple points, corresponding to maximum areas of 1400 nm^2 and generally much smaller. Under an electron

beam, those glassy intergranular regions appear to be susceptible to ionization damage, too (see Fig. 4). If we compare the micrographs with the case of Si_3N_4 we see that the contrast alterations are very similar.

(iii) Zinc oxide

In order to investigate the irradiation damage process further, a sample of "high purity" ZnO was examined. This sample also contained a glassy phase which seemed to be heterogeneously localized in some grain boundaries. The width of the glassy area is <16 nm and is generally smaller. The presence of a glassy phase indicates either that impurities such as Na, Ca or Pb segregated to the boundary regions during the forming process or that preferred reduction of zinc at the boundaries promoted glass formation. The glassy phase was again susceptible to the same characteristic ionization damage.

2.2 Bubble Growth Rate

(i) Silicon nitride

The sequence of micrographs given in Fig. 2 illustrates the nucleation and growth of bubbles at 100 kV. In Fig. 2 (a), exposed within 20 s, the glassy phase (G), which may be identified from the electron diffraction ring patterns [(Fig. 2 (d))], shows faint speckled contrast, suggesting defects have already nucleated. After 2 min in the beam of 9 A/cm^2, further growth of the bubbles is apparent and the average radius is now ~200Å [Fig. 2 (b)]. Subsequent exposure to the beam resulted in continued bubble growth, Fig. 2 (c). A corresponding plot which represents the average of many curves of bubble radius as a function of time at 100 kV is given in Fig. 5, and it is seen that an initial rapid growth rate is succeeded by a progressively slowing rate. The accuracy of the measurements is limited because the bubbles show weak contrast and are not always spherical. However,

the initial form of the growth curve which is specific in fitting an appropriate relation was reproduced in a number of experiments.

(ii) Manganese-Zinc ferrite

An example illustrating the microstructural changes after only 1 min exposure to an electron beam of 9 A/cm^2 at 125 kV is shown in Fig. 2. The rate of bubble growth was slower for the ferrite than for Si_3N_4 since the bubble radius was 25 Å after 1 min and reached 100 Å only after 15 min irradiation, which corresponds to a ratio of 1/2 if compared with bubble growth in Si_3N_4 at the same voltage. However, the form of the curve relating the bubble radius to exposure time obtained from several sequences of micrographs (Fig. 6) is similar to the Si_3N_4 curve.

(iii) Zinc oxide

The bubble growth was again very rapid as may be seen from Fig. 7: after 1 min irradiation, the bubbles reached their maximum size corresponding to the width of the glassy intergranular regions (r = 80 Å). A comparison with the growth rate for nitride and ferrite shows that the ionization damage rate in ZnO is comparable to the rate in Si_3N_4.

2.3 Voltage and Intensity Dependence of Bubble Formation

A series of experiments was performed at progressively higher accelerating voltages, namely 60, 80, 100, 125, 150, 200, 300, 400, 500, 650 and at varying electron beam intensity in the range 9-32 A/cm^2 (no aperture on the second condenser). In Fig. 8 (a,b) the growth rates of bubbles are given for voltages 100 and 60 kV for Si_3N_4. They show that the growth rate increases with the electron beam intensity and decreases with the voltage, which is characteristic of an ionization damage process. At 150 and 200 kV the incubation period for bubble nucleation was much longer and slight changes were observed only after times in excess of 15 min.

Exposure at accelerating voltages of 300 kV and higher produce no visible alterations in structure up to times of 30 min. Since the rate of damage accumulation depends on the beam characteristic of the microscope, variations between the observations on the Siemens 102, HU 650, and the works of Drew and Lewis (on a JEOL 200) are expected, and the results cannot be correlated directly.

3. Kinetics of Ionization Damage in Glassy Ceramics

When the nitride and ferrite bubble growth data presented in Figs. 8 (a,b) and 6 are plotted as r against $t^{1/2}$, reasonably good straight lines are found [(Figs. 9 (a,b) and 10)]. In Fig. 11 (a,b) the growth rates obtained from the previous figures are plotted against beam current I at constant voltage, and the inverse of accelerating voltage V at constant beam current, respectively. From the observed linear dependences it appears that the bubble growth obeys a relationship of the form $dr/dt = AI/V$, where A is a constant.

It may be noted that if an electron produces only one ionization event during its passage through the specimen, as expected from typical ionization cross sections in materials, the growth rate will be a linear function of the beam current. Moreover, since theory predicts a $1/v^2$ dependence of ionization damage on the electron velocity v, the 1/V dependence is also expected. Therefore, we may assume that the kinetics of ionization damage in glassy ceramics will follow the law: $r = \sqrt{2\ AI/V\ t}$. The reasons why bubbles are not observed in specimens irradiated for comparable times at 300 kV and above in a high voltage electron microscope is understood from the cut off voltages at 200 kV predicted from Fig. 11 (b).

4. Discussion

4.1 Ionization Damage of Matter

Previous work has indicated that gases can be evolved from glasses during exposure to an electron beam. Lineweaver[5] has shown that oxygen is evolved from an aluminum coated soda glass during electron irradiation at 20 kV. Dudek[14] has reported the formation of large gas bubbles in glass during electron beam exposure, and Yamamoto[15] has made in situ observations of bubble formation in soda glass by transmission electron microscopy. The present work provides further direct evidence that in some specific conditions fine scale precipitation of the gas can occur in glassy ceramics. It is thus clear that many different glassy materials are susceptible to ionization damage and gas bubble formation. It has been known for many years that halides undergo dramatic changes in structure when irradiated with electrons.[2] For example, Forty[3] studied PbI_2 extensively using TEM techniques and showed that iodine bubbles and metallic Pb were formed by the reaction $PbI_2 \rightarrow Pb + I_2$. In a similar way hydrogen bubbles can be created in organic compounds by breaking of the C-H bond.[16,17] A similar reaction of the type $2MO \rightarrow M + O_2$ could also account for the observations on glass. However, the formation of a bubble must be preceded by formation of free gas, which depends on the nature of the chemical bonding and interaction with radiation. Two different cases may be distinguished: (a) if the single bond-energy between the anion and cation is low (<2 eV), the energy transferred by the electron beam in an elastic collision may be sufficient to break the bond and ionize the anion to a gas atom. Two possible paths to gas bubble formation then exist. The gas can diffuse in the atomic state and agglomerate, or adjacent ions can form a gas molecule and diffuse as an entity to form a bubble. This mechanism will occur for

organic materials or halides in which the bond energy is <2 eV. (b) If the single bond energy is higher than 2 eV ion displacements are impossible at 100 kV but electron transfer between network modifier cation in a glass and its associated oxygen half-ion may free atoms and positively charged O, which may again lead to O_2 molecules formation and subsequent coalescence into gas bubbles. This is the case for alkali and alkali-earth glasses.[5]

4.2 Ionization Damage in Ceramics

We will now consider the mechanism and possible criteria for ionization damage in glassy ceramics. From the similarities in network structures and observed effects with soda glass, it seemed legitimate to analyze the ionization damage mechanism by comparison with the Lineweaver's case when Na_2O is added to pure silica. Thus a discussion of the different stages of the damage mechanism will now be given in these terms for each of the ceramics considered.

(i) Damage Nucleation

Consider first the case of vitreous silica.[18] The structure is such that each oxygen is covalently bonded to two silicon atoms and all the valency electrons are shared in strongly directional bonds[19,20] (of bond strength = 4.6 eV). Oxidation of an oxygen by ejection of an electron from the L shell is precluded by this high bond energy. Thus pure vitreous silica, like most semiconductors will be insensitive to ionization damage. On the other hand if Na_2O is added to the structure and is dispersed in the lattice homogeneously we may postulate that a dangling $Si\text{-}O^-$ bond will form.[18] This configuration will be more susceptible to beam-induced changes since the electrons will have the tendency to reduce Na^+ to Na^o by electron transfer from O^o. The remaining electron on O^- will be easier to remove, as according to the spectroscopic data,[21] the bond energy is reduced by

20%. An atom of oxygen will thus be created simultaneously. A similar process is likely to occur when MgO or CaO are added to Si_3N_4 or ferrites as it is schemed in Fig. 12 (a,b). In both cases three effects will combine to increase the probability that a configuration susceptible to ionization forms: (1) non-bridging oxygens, (2) impurity segregation, which leads to high local Ca or Mg concentrations in the glassy phase in grain boundary regions, and (3) shortening of bonds. Etchepare has shown that the O-O bond length varies in an alkali or alkali earth glassy phase and that it can be shorter than the O-O crystalline bond.[22]

(ii) Bubble Growth

If the concentration of network modifying cation is sufficient, the glass structure becomes more open and we can assume that the case is similar to alkali glass and that, in agreement with the bubble contrast observed in electron microscopy, bubbles are formed by agglomeration of atomic, molecular or ionized oxygen. Since the solubility of oxygen in solid glass is low (typically 10^{-4}), the gas supersaturates rapidly during the irradiation creating conditions favorable for bubble nucleation and growth. In order to explain the rapid growth of bubbles it is necessary to invoke a large diffusion coefficient for oxygen in glass. Diffusion over the order of 500 Å in 30 s is required, i.e., $x = 5 \times 10^{-6} = 30\ D$, or $D \simeq 10^{-12}$ cm^2 sec^{-1}. From the available diffusion data for oxygen in glasses,[23] it is seen that even the largest reported values, when extrapolated to the estimated glass temperature of 150-200°C (Ref. 24), indicates $D \sim 10^{-15}$ cm^2/sec^{-1}. Thus an alternate explanation for the fast diffusion is required. The spectroscopic data obtained by energy loss[25] suggest an answer, since it has been shown that the oxygen peak observed at ≃30 eV from an incident electron beam of 25 kV arises from an ionized oxygen

molecule (O_2^+) corresponding to a scattering angle of 0.5° at 125 kV. Since the size of the O_2 molecule is greatly reduced by ionization a considerable enhancement in diffusion rate through the glass network is predicted upon ionization even if the rate of recombination of O_2^+ under the electron beam is high.

A theory to describe bubble formation in non-crystalline solids does not appear to have been formulated, but the case of gas bubble growth and dissolution in molten glass has been treated by Doremus,[26] while Greenwood et al.[27] have derived equations for inert gas bubble nucleation and growth in crystalline solids during neutron irradiation. If the growth rate is limited only by mass transport from the bubble, the extreme case of Greenwood et al. equation (6) may apply, viz., $dr/dt = DvCo^v/r$, where Dv is the vacancy diffusion coefficient and Co^v the actual vacancy concentration. It follows that $r = (2DvCo^vt)^{1/2}$, showing a square root dependence of bubble radius with time. This relation can be compared with that derived by Doremus for a shrinking gas bubble in molten glass which also shows the same dependence; $r = (2\beta Dt)^{1/2}$ where D is now the gas diffusion solubility and β is related to the gas concentration in the bubble, matrix, and interface. It is noticeable that the bubble growth in electron-irradiated glassy ceramics seems to correspond to the same square root of time dependence as in molten glass or in neutron irradiated crystalline solids. A full theory of the bubble growth would be of interest to understand the growth mechanism and its implication on the structure of the glassy phase.

(iii) Influence of the Oxidation State of the Network Modifying Cation

Since bubble nucleation and growth occurs only when the glass becomes supersaturated with free oxygen, the absence of bubbles in some glasses implies the O_2 liberation has been inhibited. This result can be understood

from the effects of other impurity interactions in the glass structure. For example, if polyvalent cations are also present in the neighborhood of the liberated oxygen, O will be immediately reduced and re-dissolved in the lattice by an oxidation-reduction of the type $M^{n+} + O \rightarrow M^{(n+1)+} + O^{-}$ (II). This effect is analogous to that proposed by Greene et al.[28] to account for the finning of glasses by selected impurity-additions.

(1) In the case of Si_3N_4, the network modifiers, Ca and Mg, are not polyvalent; therefore, the reduction of free oxygen according to equation 2 is impossible.

(2) In the Mn-Zn ferrite the situation is more complex since several of the ions present are polyvalent. The behavior in the glassy intergranular phase will depend on which ions have segregated to the grain boundary. We may assume that there is a strong segregation of Ca^{2+} (>15%) at the grain boundaries.[17] On the other hand the Fe^{2+} concentration is small (>1.5%) and Sn^{2+} concentration should be small too, since Sn^{4+} is soluble in the matrix. Therefore the relative concentrations of the potentially reducing cations Fe^{2+} and Sn^{2+} will be too low to allow the reduction of free oxygen.

(3) Since the ZnO studies was prepared from pure materials, the polyvalent impurity level should be low. Moreover, if it is accepted that the glassy phase at the grain boundaries arises from an excess of Zn as a result of firing in a reducing atmosphere, reduction of the Zn will be favored over reduction of the oxygen to preserve charge neutrality and free oxygen liberation again occurs.

II. CONCLUSION

A mechanism of ionization damage in ceramics is proposed which is compatible with the mechanism of Lineweaver for outgassing from an aluminum-coated alkali glass. The nucleation of bubbles under the electron beam depends on the presence of non-bridging oxygen, and bubble growth will occur if the ratio of polyvalent cations to non-bridging oxygens is low enough. Thus, such ionization damage is likely to occur in glassy oxide phases formed with cations such as alkalis and alkali-earths and Ag, Au, Zn and Cd. This effect is not likely to occur with transition elements which can easily change their oxidation state and reduce oxygen.

The effect should also occur with glassy phases formed with anions having an electro-negativity higher than, or comparable to oxygen, i.e., with halides or with nitrogen and sulphur. This possibility will be considered in more detail in a subsequent paper in which the structure and the chemical bonding of glassy phases in ceramics is considered.

Acknowledgments

We wish to thank Prof. R. H. Doremus for many useful suggestions and advice. A French Government fellowship is greatly acknowledged by J. Y. Laval. This work was partially supported by the Division of Materials Science, Office of Basic Energy Sciences, U. S. Department of Energy under Contract W-7405-ENG-48.

References

1. "Short Wavelength Microscopy," Annals of the New York Academy of Sciences 306, 85-156 (1978).
2. L. W. Hobbs, "Transmission Electron Microscopy of Extended Defects in Alkali Halide Crystals" in Surface and Defect Properties of Solids,

Vol. 4 (1975), A Specialist Periodical Report--The Chemical Society, London.

3. A. J. Forty, "The Precipitation of Lead During Decomposition of Lead Iodide by Electron Irradiation," Phil. Mag. 6, 895-905, (1961).
4. D. L. Griscom, "E.S.R. Studies of Radiation Damage and Structure in Oxide Glasses Not Containing Transition Group Ions: A Contemporary Overview With Illustrations From the Alkali Borate System," 13, 251-285 (1973).
5. Jack L. Lineweaver, "Oxygen Outgassing Caused by Electron Bombardment of Glass," J. of Appl. Phys. 34, [6] 1786-1791 (1963).
6. Tennyson Smith, "Auger Electron Spectroscopy and Ion Sputter Profiles of Oxides on Aluminum," Surf. Sci. 55 601-624 (1976).
7. L. Tertian, D. Hokim and J. P. Riviére, "Transformations in Thin Foils of Cuprous Oxide as observed in an Electron Microscope," J. Phys., 39, 1135, Paris, October 1978.
8. P. Drew, M. H. Lewis, "The Microstructures of Silicon Nitride Ceramics During Hot-Pressing Transformations," J. of Mat. Sci., 9, 261-269 (1974).
9. M. H. Lewis, B. D. Powell, P. Drew, R. J. Lumby, B. North, A. J. Taylor, "The Formation of Single-Phase Si-Al-O-N Ceramics," J. Mat. Sci. 12, 61-74 (1977).
10. J. Makin, private communication.
11. A. Hamelin, "Segregation at Grain Boundaries in Manganese Ferrites," Ph. D. Thesis in Physical Sciences, University of Paris, Orsay, France, 1972.

12. M. Paulus, pp. 453-73 in Microstructural Science, Vol. 3. Edited by P. M. French, R. J. Gray and J. L. MacCall. American Elsevier, New York, 1975.

13. P. B. Hirsch, A. Howie, R. B. Nicholson, D. W. Pashley, M. J. Whelan, "Electron Microscopy of Thin Crystals." 1965, Butterworths, Washington.

14. Von Hans Joachim Dudek, "Blasenbildung in Glass bei Electronenbestrahlung," Glastechn, Ber.-41, [1], 10-12.

15. Tokuji Yamamoto, Sumio Sakka and Megumi Tashiro, "Formation of Defects in Glass Under Electron Bombardment," J. Am. Ceram. Soc. 55, [9], 473-474 (1972).

16. M. A. Slifkin and Y. M. Suleiman, "A Novel Bubble Phenomenon Occurring on Electron Scanning of Amino Acids and Their Quinone Complexes," Chem. Phys. Lett. 44, [3], 586-588 (1976).

17. Walter Gordy, "Free Radicals from Biological Purines and Pyrimidines," Annals of the New York Academy of Sciences. 158, 100 (1969).

18. R. Doremus, "Glass Science" 1973, Wiley-Interscience.

19. K. J. Jack, "Review--Sialons and Related Nitrogen Ceramics" J. Mat. Sci., 11, 1135-1158 (1976).

20. W. D. Kingery, H. K. Bowen, D. R. Uhlmann, "Introduction to Ceramics" 1960 2nd Edition, Wiley-Interscience.

21. C. Dodd and G. L. Glen, "Studies of Chemical Bonding in Glasses by X-Ray Emission Spectroscopy," J. Am. Ceram. Soc., 53, [6], 322-325 (1970).

22. J. Etchepare, "Study by Raman Spectroscopy of Crystalline and Glassy Diopside," 35, 337-346 (1970).

23. R. Terai and R. Hayami, "Ionic Diffusion in Glasses," J. of Non-Crystalline Solids, 18, 217-264 (1975).

24. H. Bach, "Determination of Bond Energy of Silica Glass by Means of Ion Sputtering Investigations," Nucl. Instru. Meth. 84, 4-12 (1970).

25. J. S. Lee, "Observation of New Electronic Transitions in O_2, CO, NO, CO_2 and N_2O," J. Chem. Phys. 67, [9], 3998-4003 (1977).

26. R. Doremus, "Diffusion of Oxygen from Contracting Bubbles in Molten Glasses," J. Am. Ceram. Soc. 43, 655-661 (1960).

27. G. W. Greenwood, A. J. E. Foreman and D. E. Rimmer, "The Role of Vacancies and Dislocations in the Nucleation and Growth of Gas Bubbles in Irradiated Fissile Material" J. of Nucl. Mat., 4, 305-324 (1959).

28. C. H. Greene and A. Lee Haynes, Jr., "Effect of As_2O_3 and $NaNO_3$ on the Solution of O_2 in Soda-Lime Glass," J. Am. Ceram. Soc., 48, [1], 528-533, (1965).

Table 1. Starting composition and heating treatment of the nitride, spinel, and oxide ceramics.

	Si_3N_4	Ferrite MnZn	ZnO
Starting composition (weight %)	additives Mg 1.25 Al 2.5 Fe 0.5 Ca 0.25 others < 0.03	Fe_2O_3 52.8 MnO 29.6 ZnO 16.7 $CaCO_3$ 0.2 SnO_2 0.7	impurities Fe 10 p.p. Pb 10 p.p.
Heating treatment	sintered	sintered at 1280°C, 2 h in an oxygen atmosphere slow coating	sintered in a reducing atmosphere

FIGURE CAPTIONS

Fig. 1. Ionization damage in a MgO fluxed silicon nitride irradiated by 100 keV electrons.

Fig. 2. Electron-induced nucleation and growth of bubbles in silicon nitride. a) t = 20 s., b) t = 2mn, c) t = 5 mn, and d) microdiffraction on the glassy phase.

Fig. 3. Stereo-pair of micrographs of an irradiated area.

Fig. 4. Ionization damage in a CaO fluxed Mn-Zn ferrite electron-irradiated at 125 keV. a) exposure time, t = 0; b) t = 1 mn.

Fig. 5. Bubble growth rate at 100 keV in silicon nitride (each symbol corresponds to an average of a growth experiment data).

Fig. 6. Bubble growth rate at 125 keV in Mn-Zn ferrite.

Fig. 7. Ionization Damage in zinc oxide electron-irradiated at 125 keV. a) t = 0; b) t = 1 mn.

Fig. 8. Variation of the growth rates of bubbles with the electron beam density in Si_3N_4. a) 100 keV; b) 60 keV.

Fig. 9. Bubble growth rate in Si_3N_4 as a function of the square root of time for different electron beam densities. a) 100 keV; b) 60 keV.

Fig. 10. Bubble growth rate in Mn-Zn ferrite as a function of the square root of time.

Fig. 11. Bubble growth rate in Si_3N_4 as a function of: a) electron beam density and b) the inverse of accelerating voltage.

Fig. 12. Schematic representation of: a) silicon oxynitride structure and b) modification produced by addition of CaO or MgO: $Si-O^-$ dangling bonds are created.

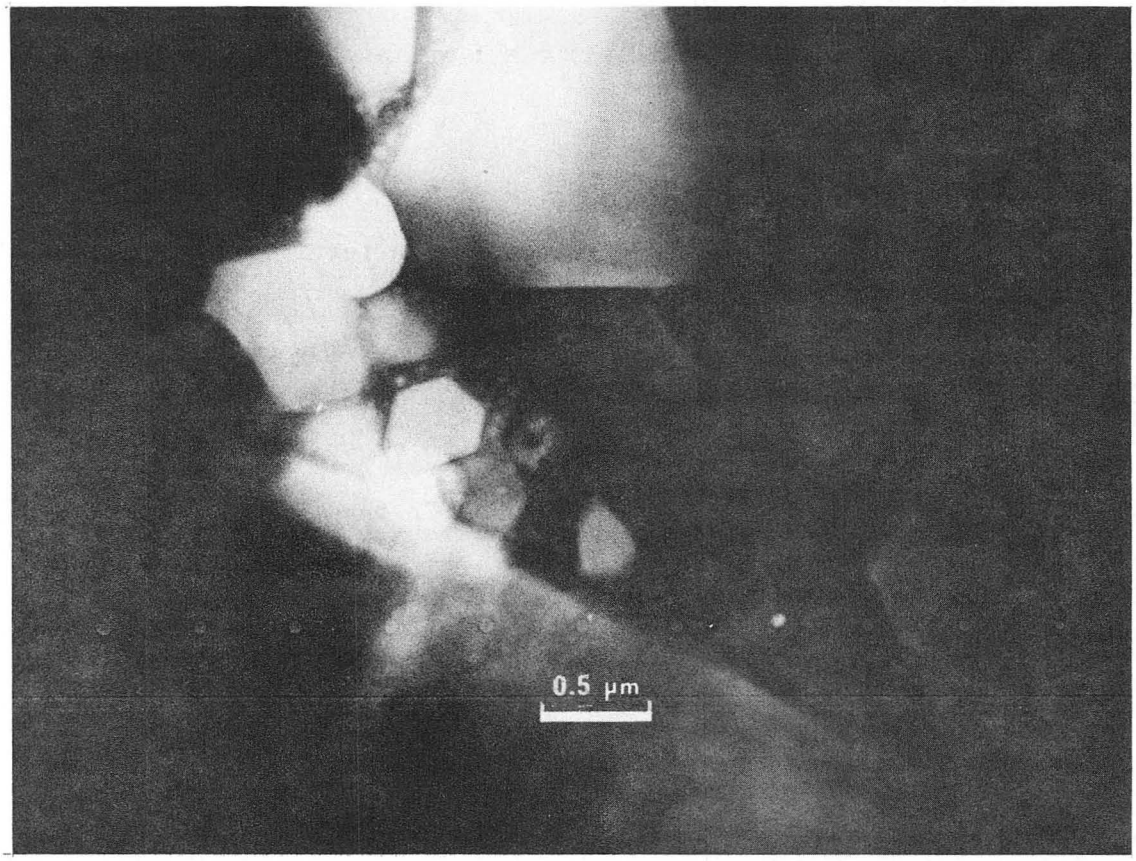

XBB 784-4340A

Fig. 1

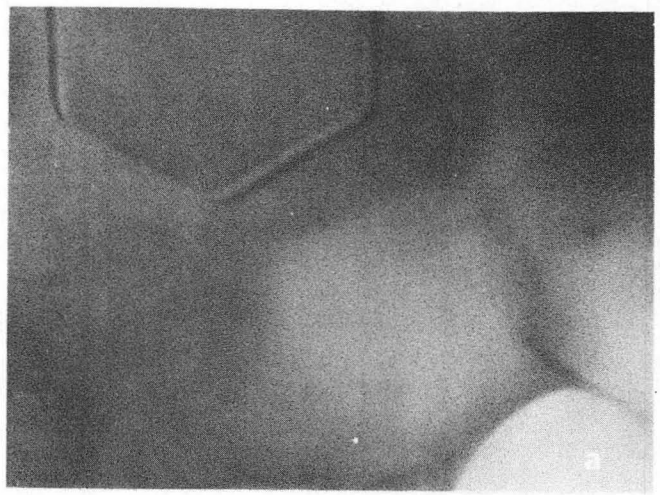

(a)

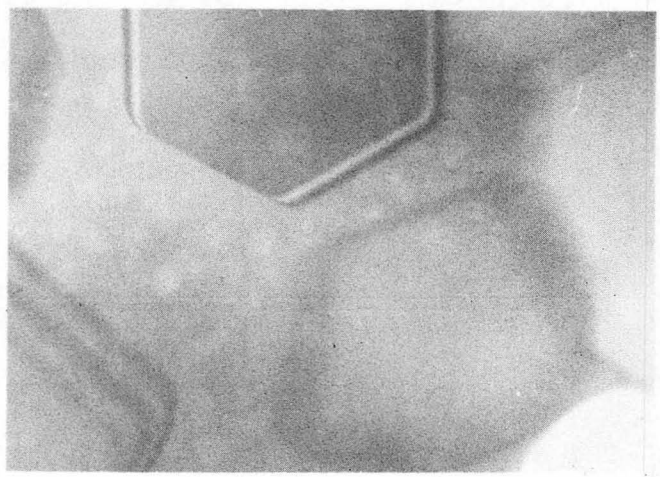

(b)

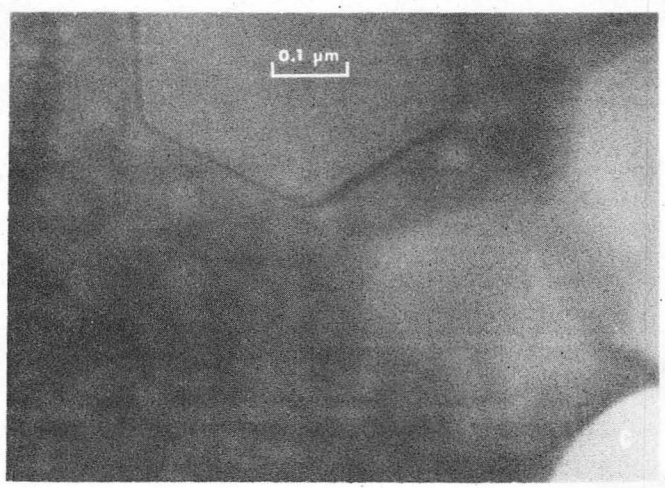

(c)

XBB 791-500

Fig. 2

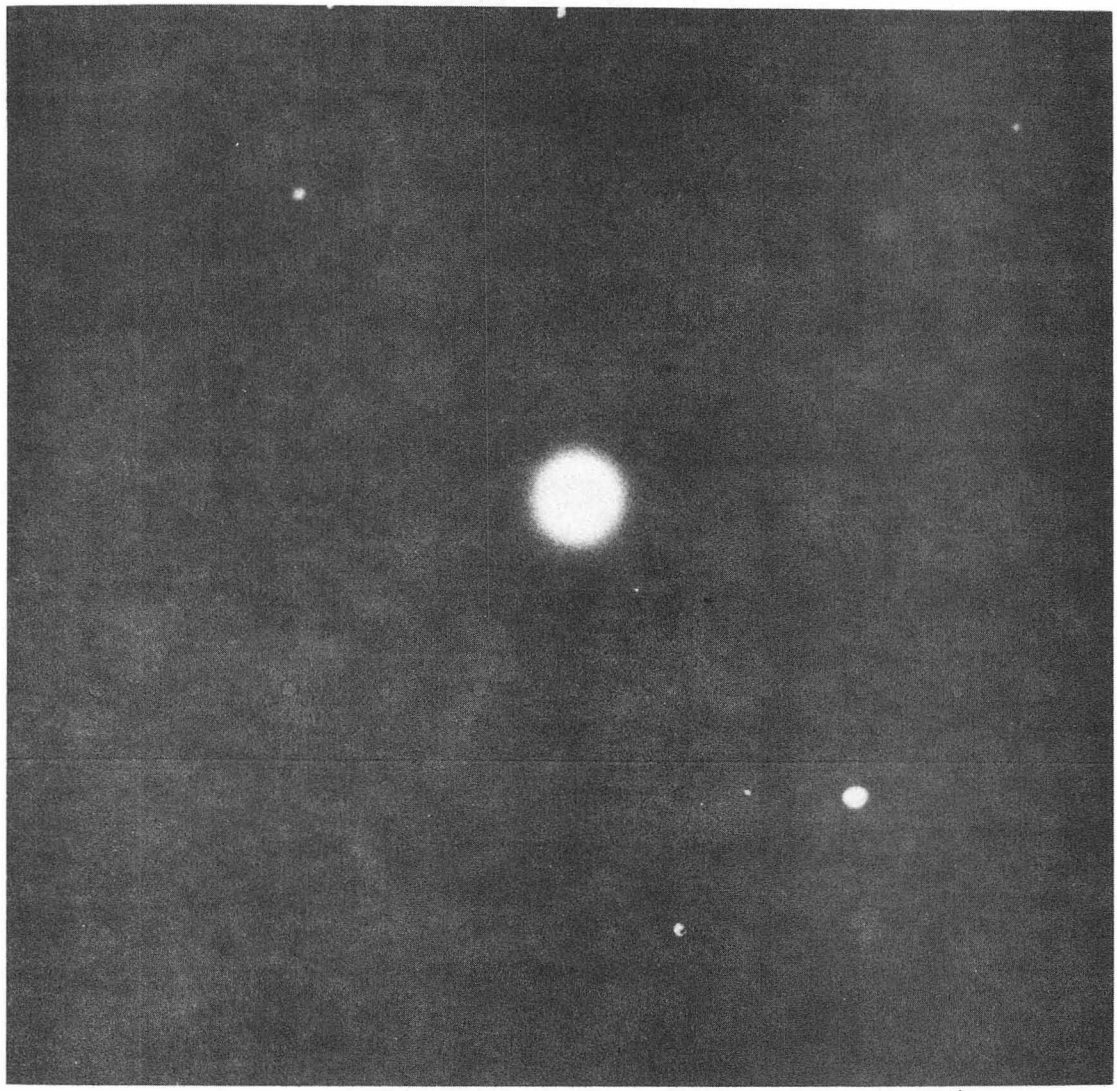

XBB 797-8913

Fig. 2d

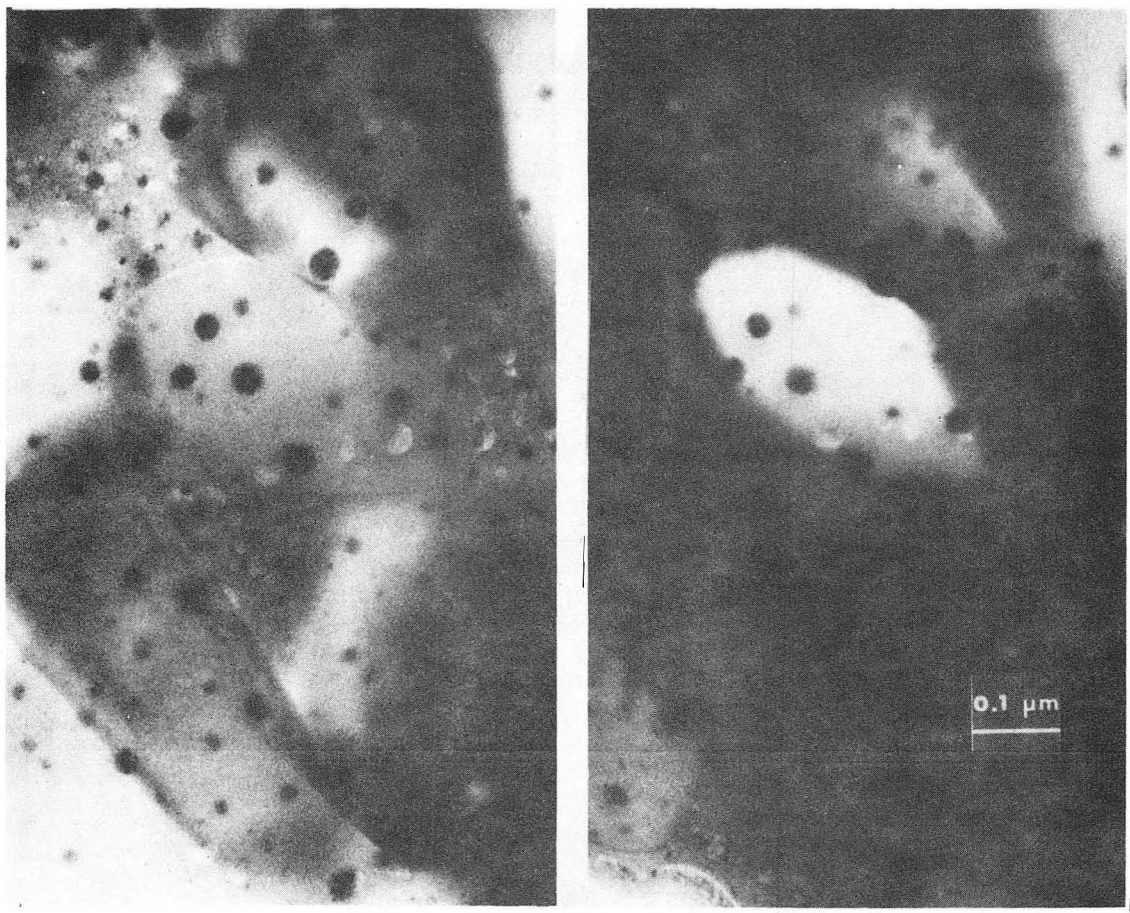

XBB 797-8914

Fig. 3

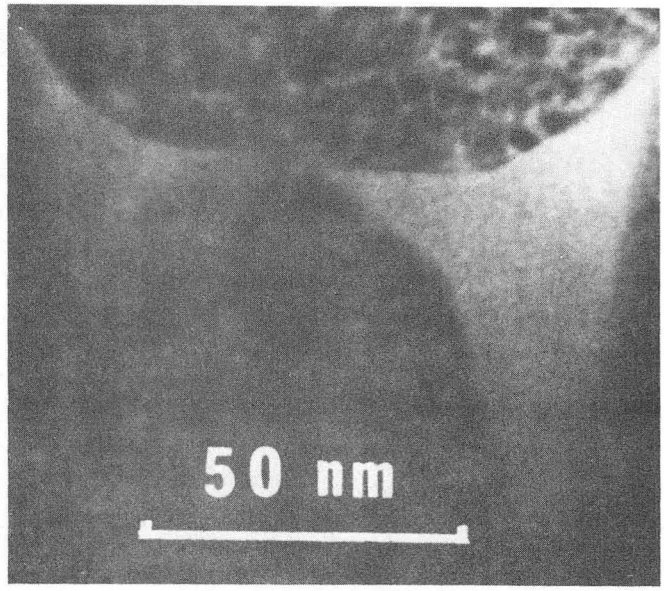

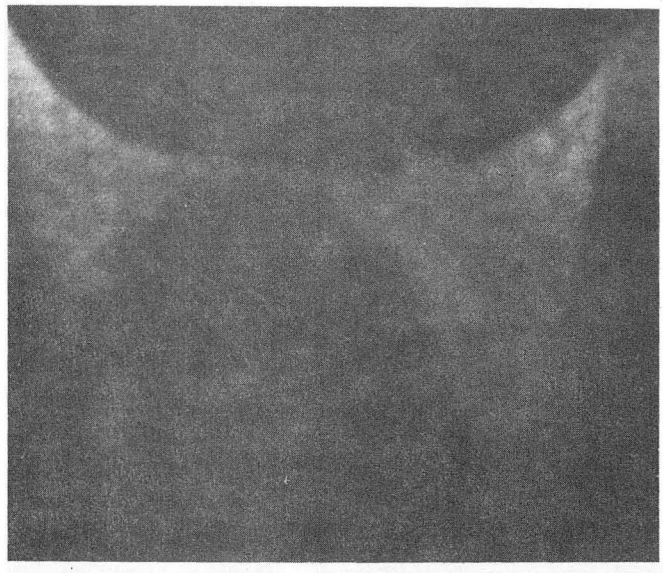

XBB 780-13433A

Fig. 4

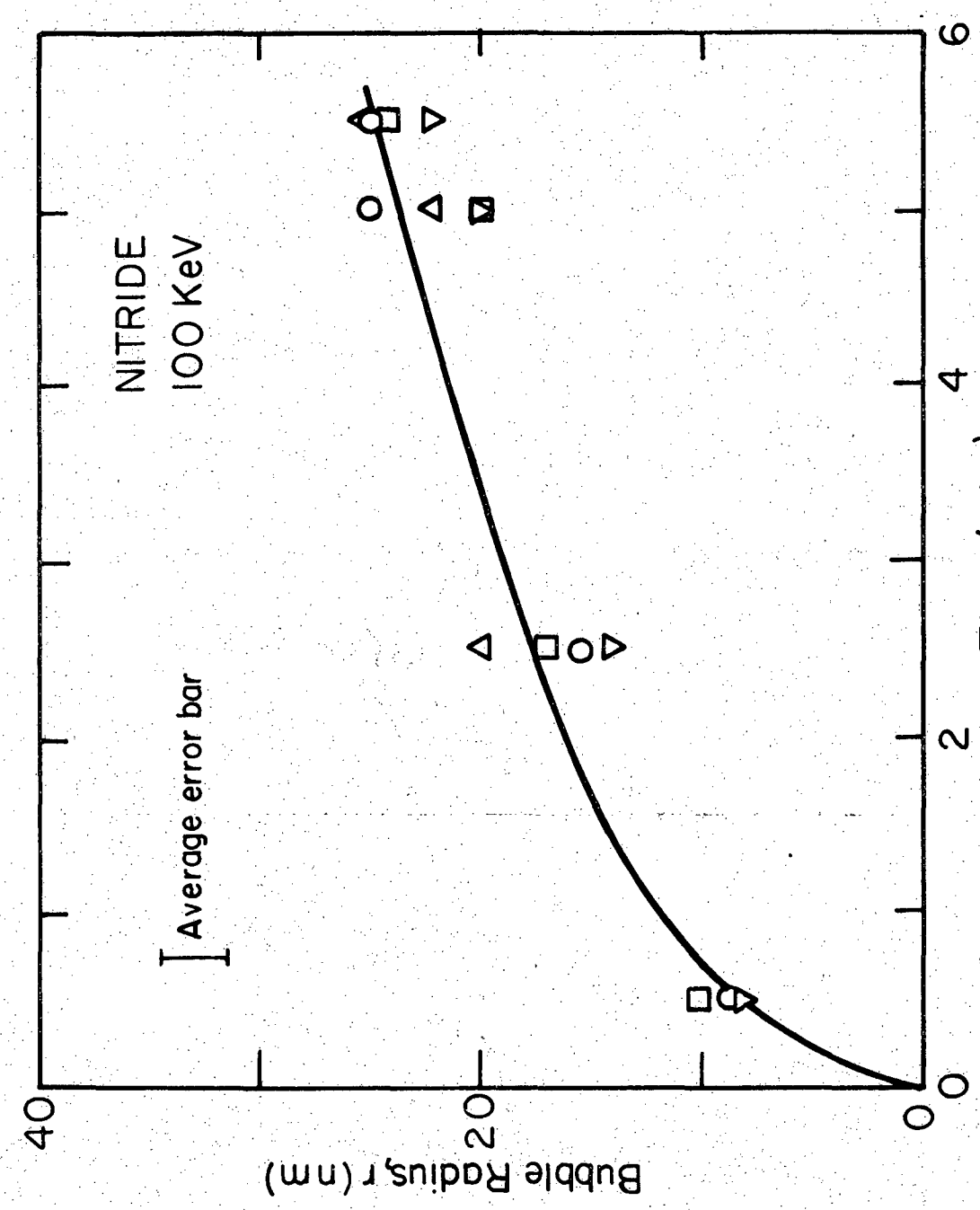

XBL 792-5790

Fig. 5

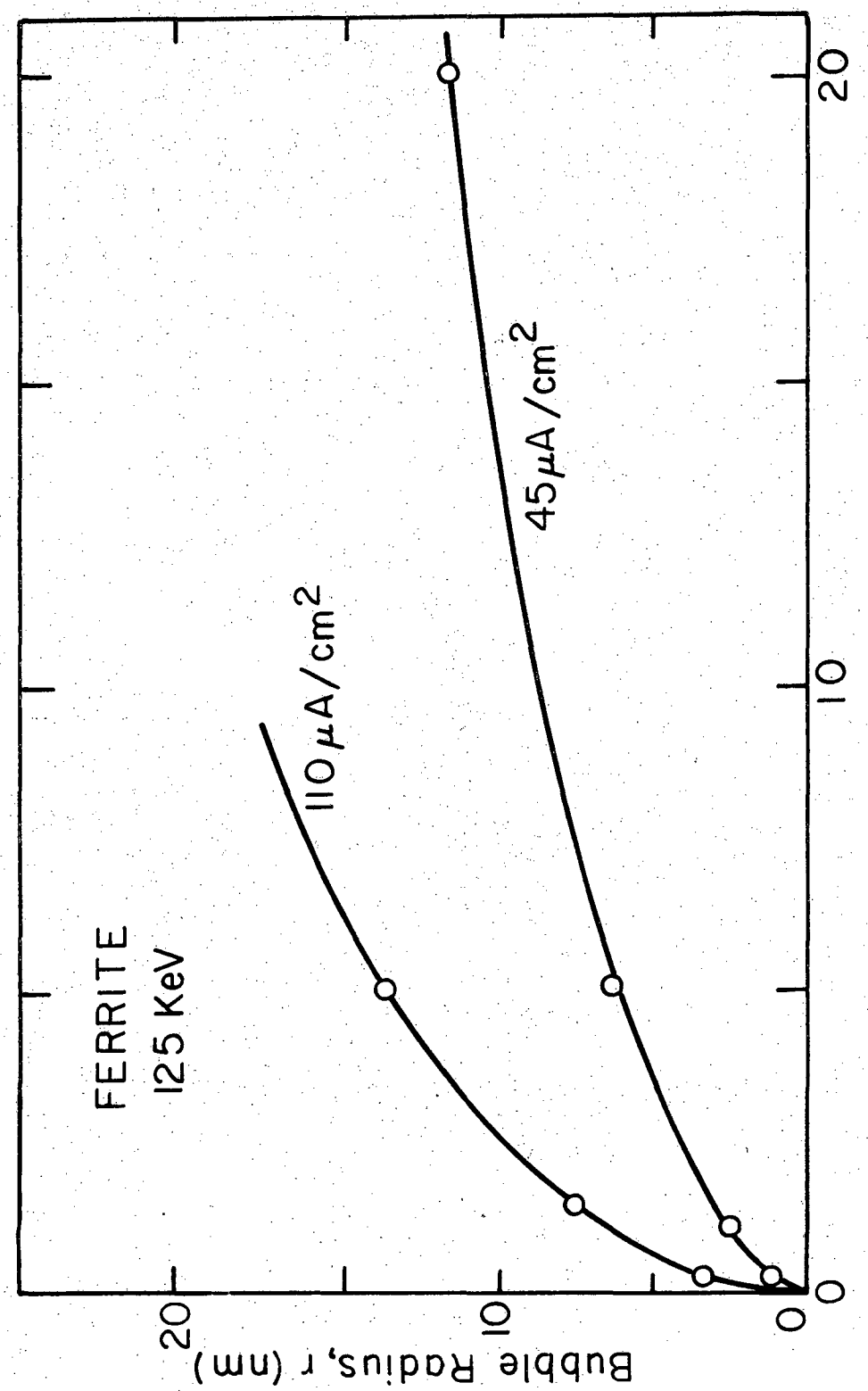

XBL 792-5797

Fig. 6

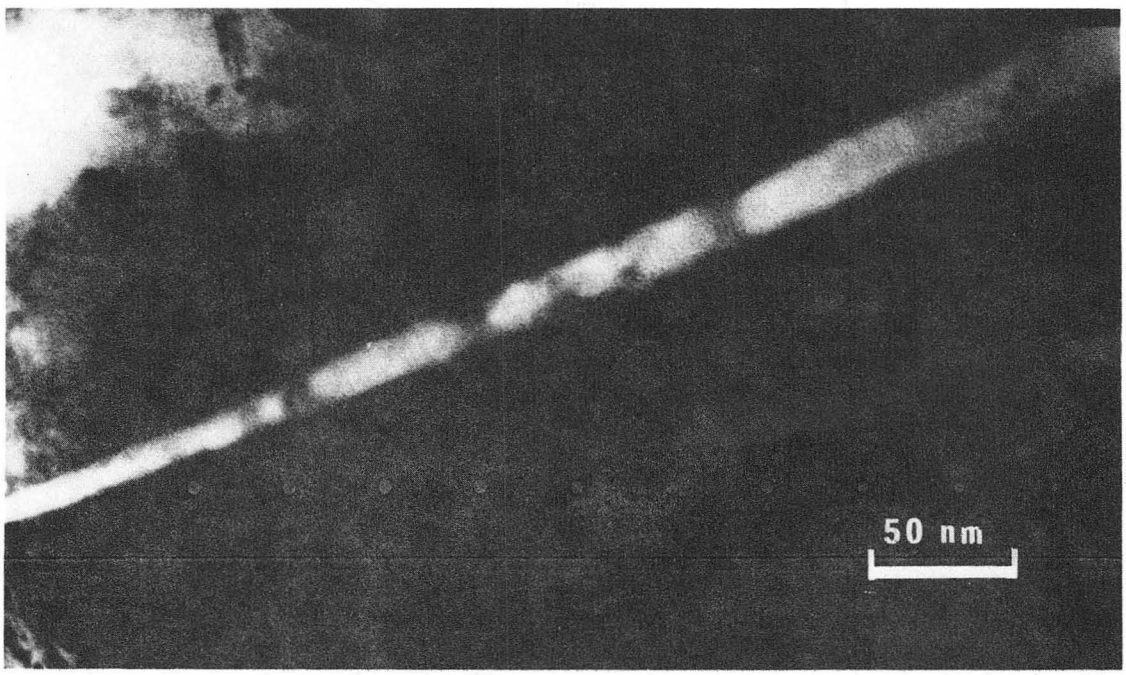

XBB 792-2165A

Fig. 7

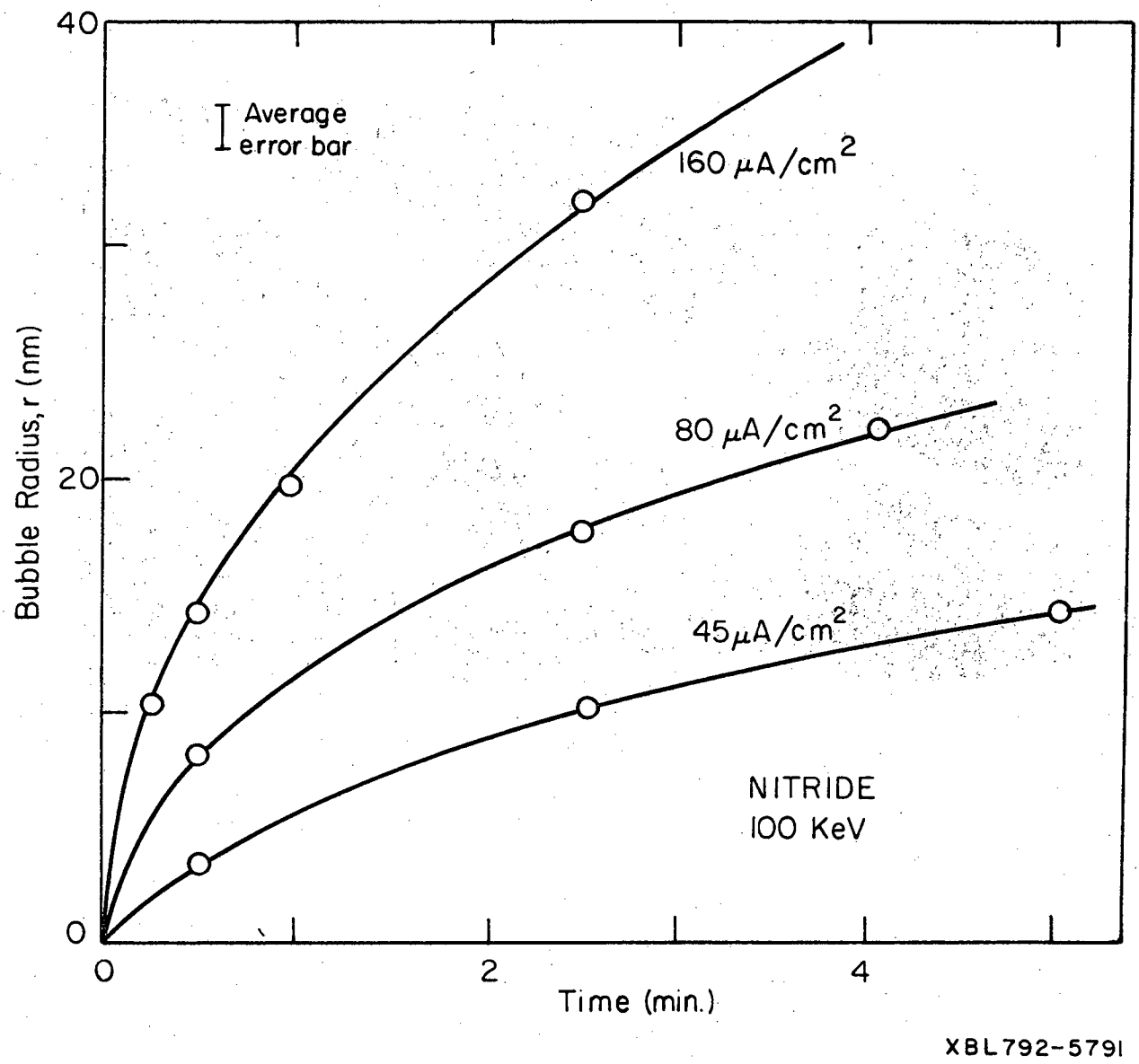
40
20
0
0
2
4
Bubble Radius, r (nm)
Time (min.)
Average error bar
160 μA/cm²
80 μA/cm²
45μA/cm²
NITRIDE
100 KeV
XBL792-5791

Fig. 8a

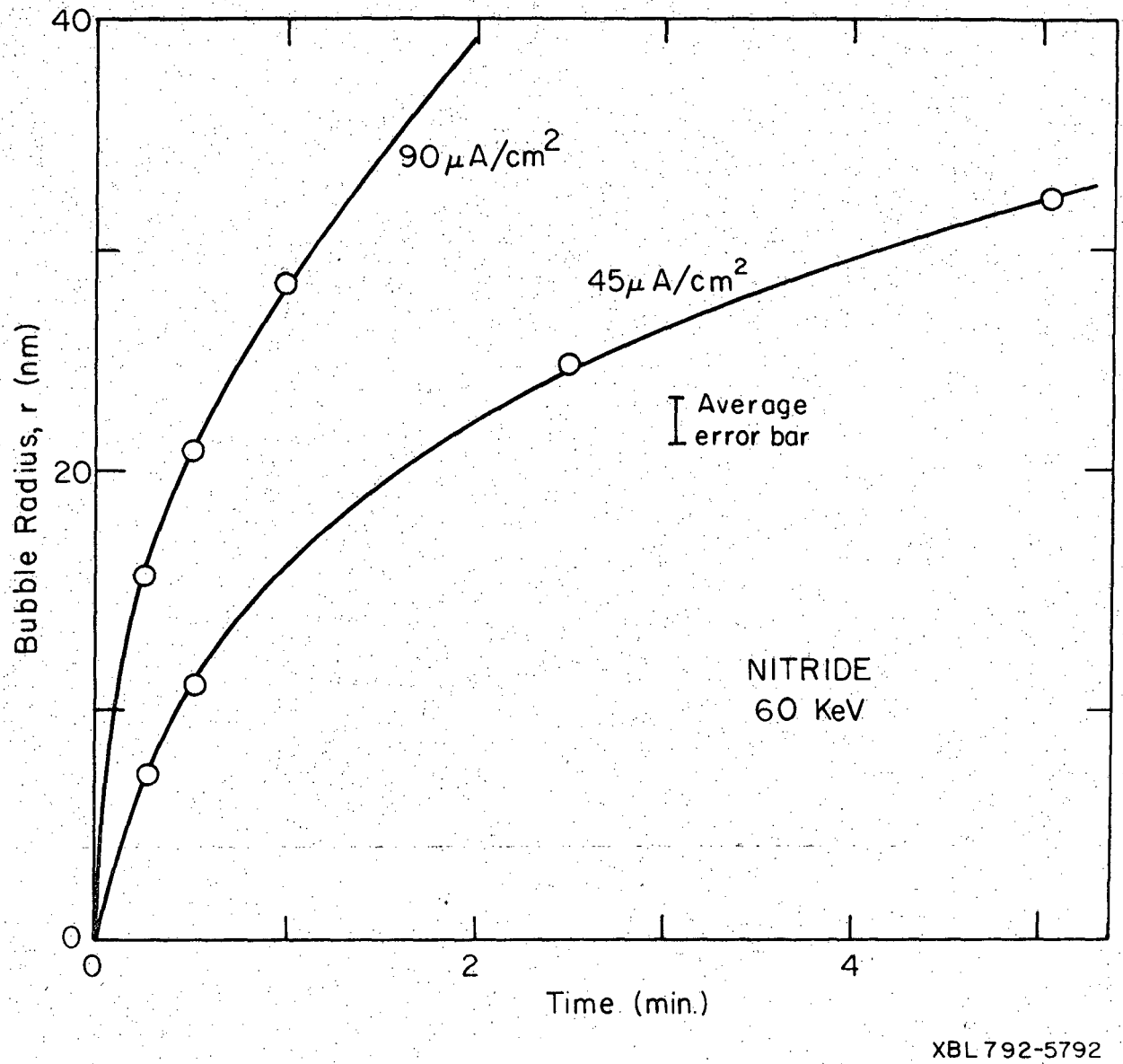
40
20
0
0
2
4
Bubble Radius, r (nm)
Time (min.)
90 μA/cm²
45 μA/cm²
Average
error bar
NITRIDE
60 KeV
XBL 792-5792

Fig. 8b

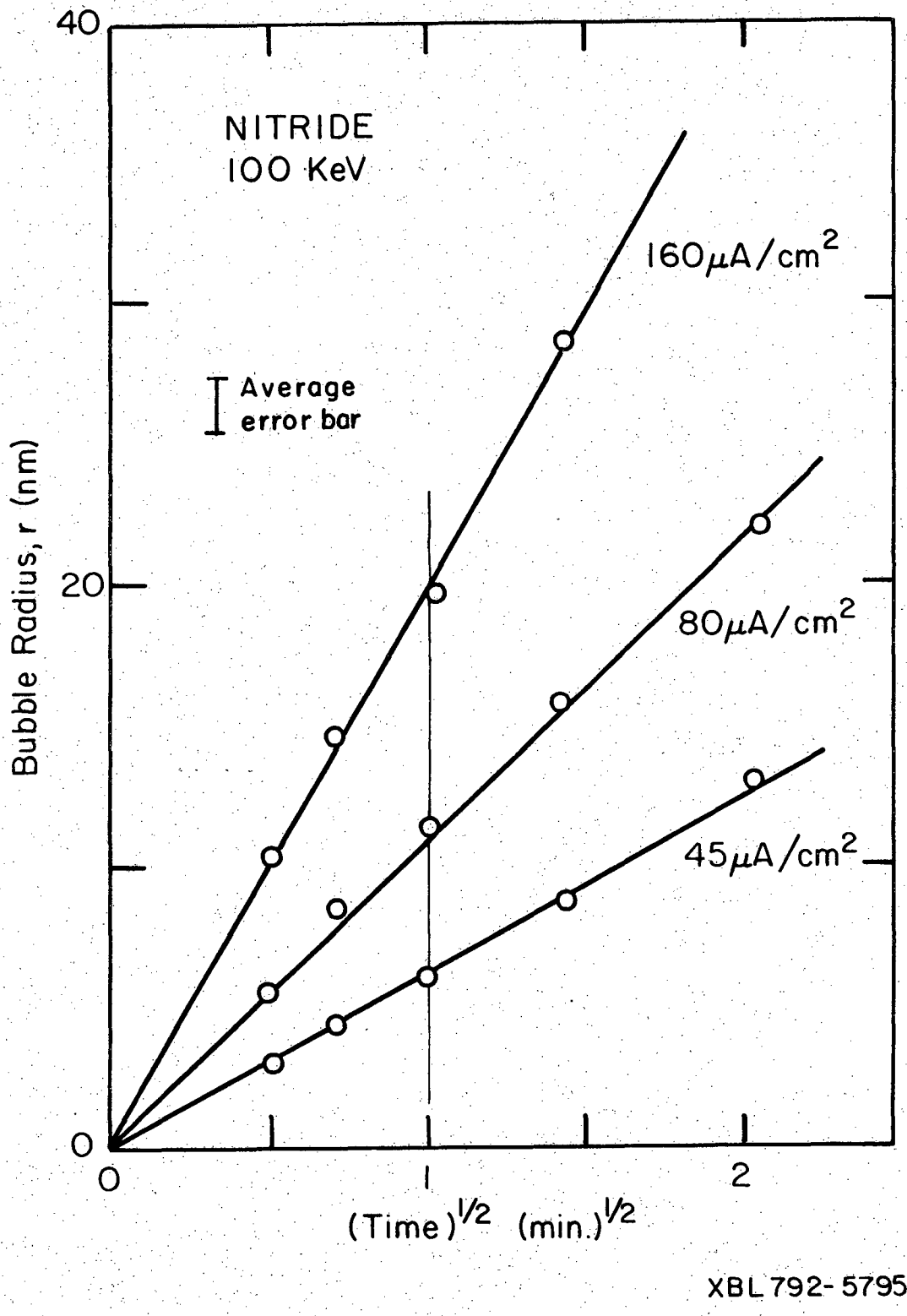
NITRIDE
100 KeV
160μA/cm²
80μA/cm²
45μA/cm²
Average error bar
Bubble Radius, r (nm)
40
20
0
0
1
2
(Time)^1/2 (min.)^1/2
XBL 792-5795

Fig. 9a

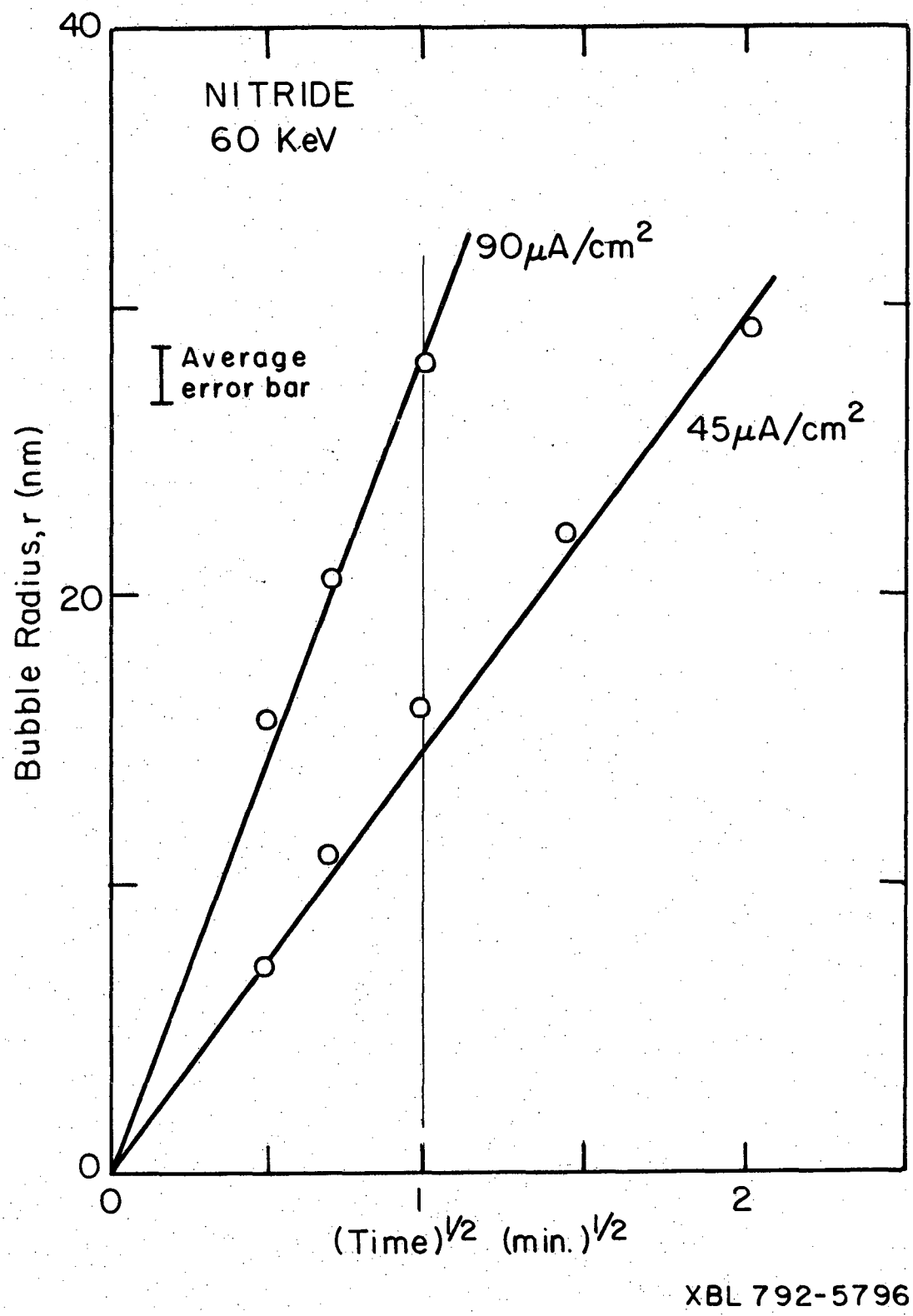
NITRIDE
60 KeV
90μA/cm²
45μA/cm²
Average error bar
Bubble Radius, r (nm)
40
20
0
0
1
2
(Time)^1/2 (min.)^1/2
XBL 792-5796

Fig. 9b

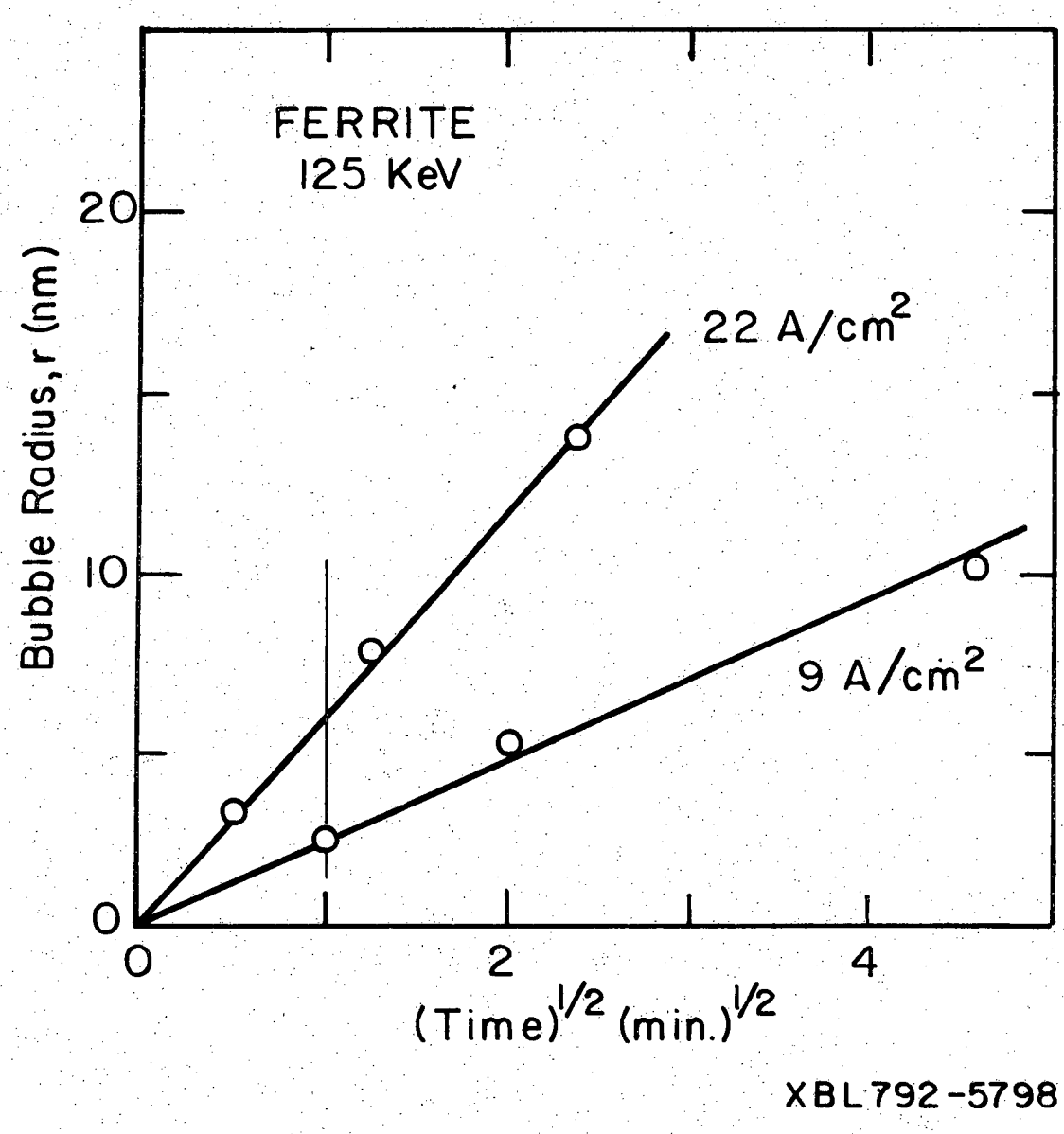
FERRITE
125 KeV
22 A/cm²
9 A/cm²
Bubble Radius, r (nm)
0
10
20
0
2
4
(Time)^1/2 (min.)^1/2
XBL792-5798

Fig. 10

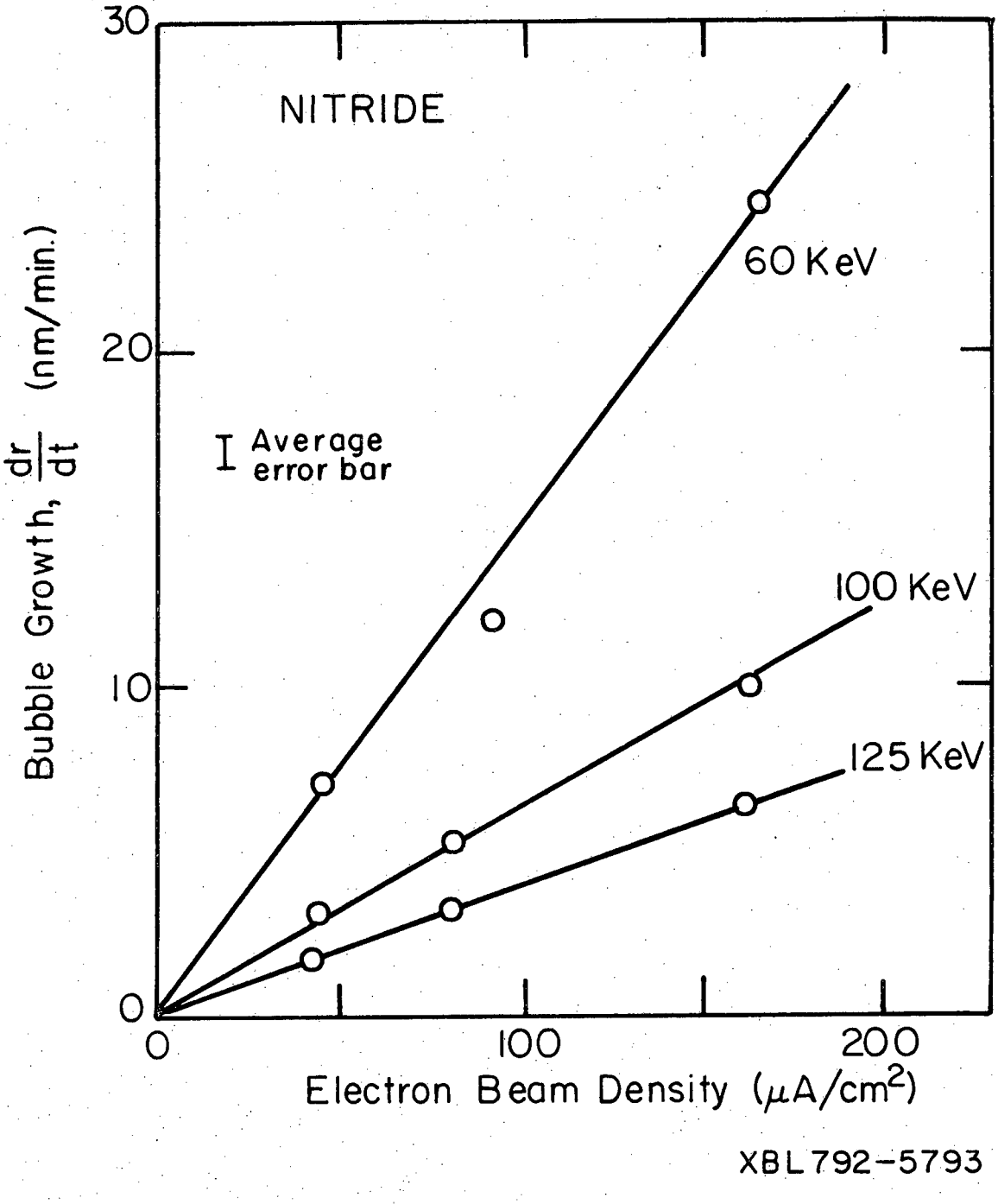
NITRIDE
60 KeV
100 KeV
125 KeV
Average error bar
Bubble Growth, dr/dt (nm/min.)
Electron Beam Density (μA/cm²)
0
10
20
30
0
100
200
XBL792-5793

Fig. 11a

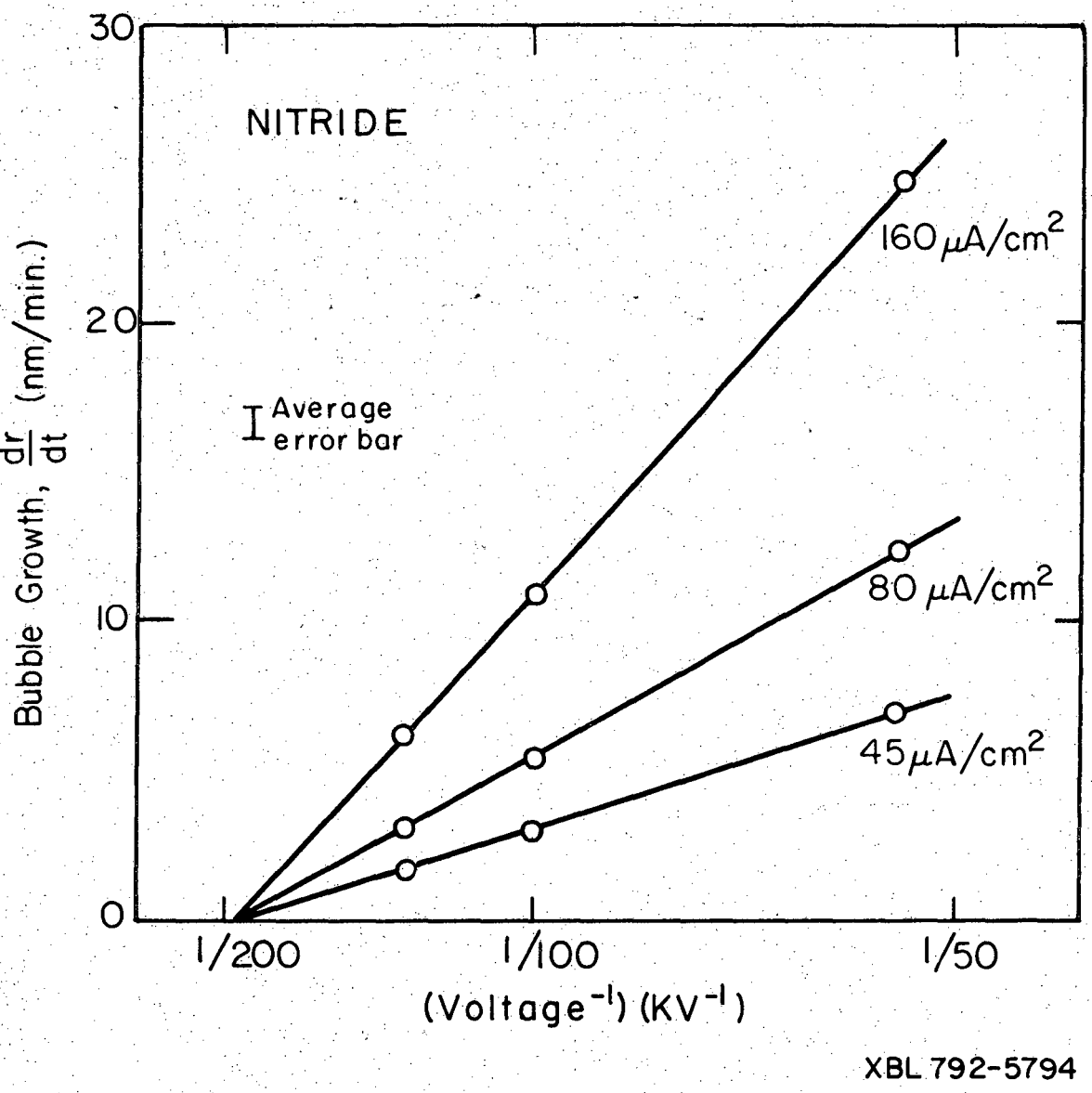
NITRIDE
160 μA/cm²
80 μA/cm²
45 μA/cm²
Average error bar
Bubble Growth, dr/dt (nm/min.)
30
20
10
0
1/200
1/100
1/50
(Voltage⁻¹) (KV⁻¹)
XBL 792-5794

Fig. 11b

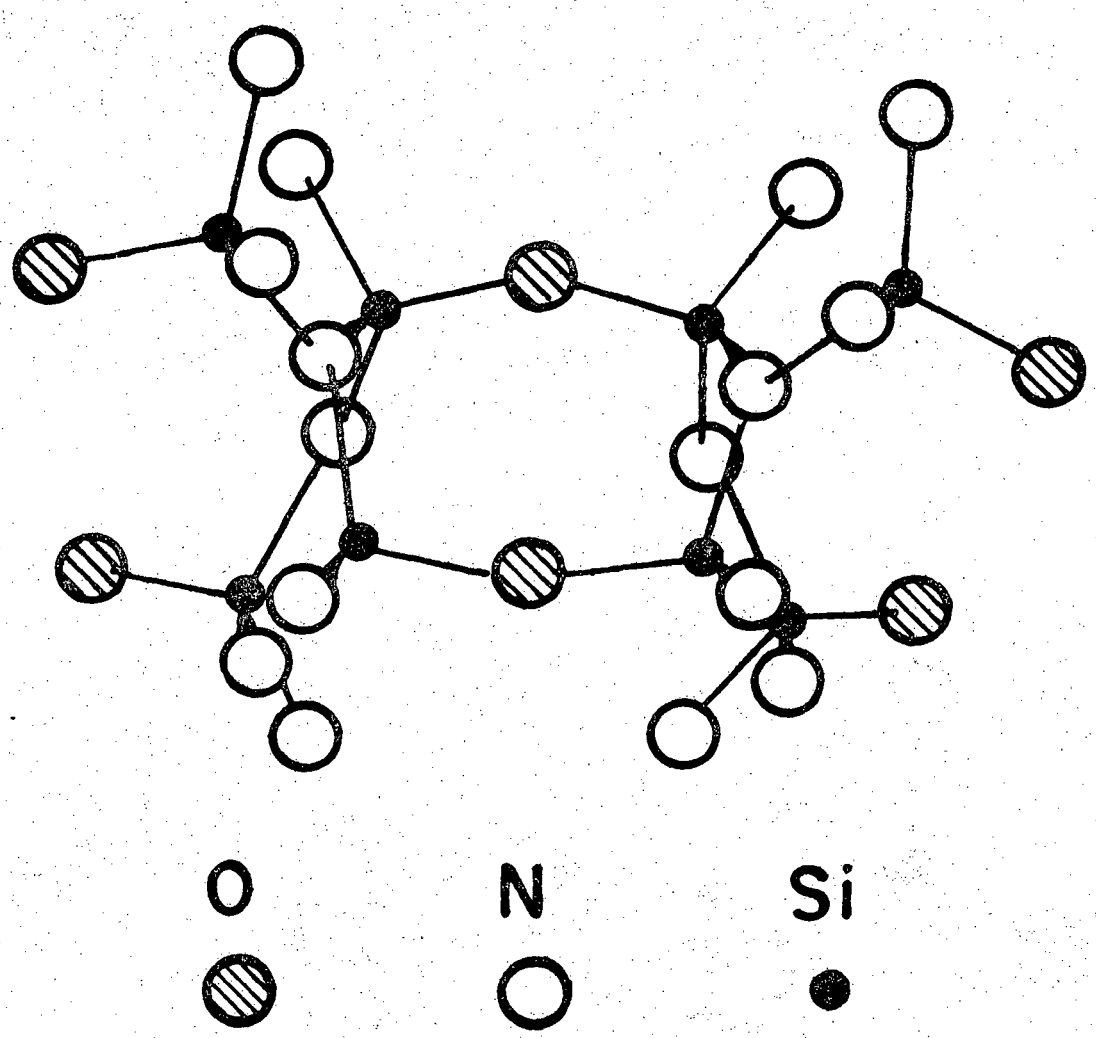

XBL 7811-6197A

Fig. 12a

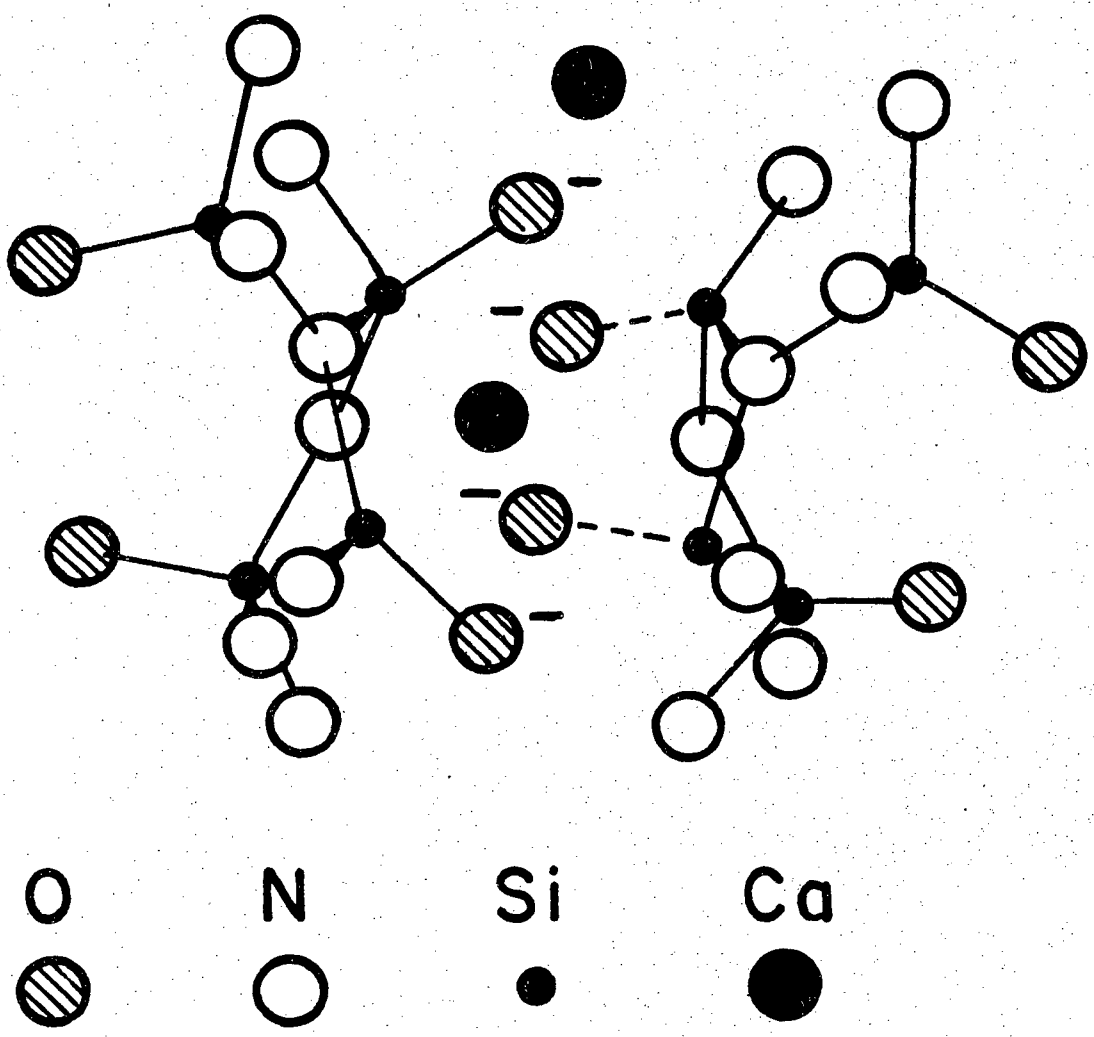

Fig. 12b

This report was done with support from the Department of Energy. Any conclusions or opinions expressed in this report represent solely those of the author(s) and not necessarily those of The Regents of the University of California, the Lawrence Berkeley Laboratory or the Department of Energy.

Reference to a company or product name does not imply approval or recommendation of the product by the University of California or the U.S. Department of Energy to the exclusion of others that may be suitable.

TECHNICAL INFORMATION DEPARTMENT
LAWRENCE BERKELEY LABORATORY
UNIVERSITY OF CALIFORNIA
BERKELEY, CALIFORNIA 94720